Size and Concentration Determination of Colloidal Nanocrystals by Small-Angle X-ray Scattering

Jorick Maes, Nicolo Castro, Kim de Nolf, Willem Walravens, Benjamin Abécassis, Zeger Hens

Size and Concentration Determination of Colloidal Nanocrystals by Small-Angle X-Ray Scattering

Jorick Maes,[†,‡] Nicolo Castro,[¶] Kim De Nolf,[†,‡] Willem Walravens,[†,‡] Benjamin Abécassis,[*,¶,§] and Zeger Hens[*,†,‡]

[†]*Physics and Chemistry of Nanostructures (PCN), Ghent University, Ghent, Belgium*

[‡]*Center for Nano and Biophotonics, Ghent University, Ghent, Belgium*

[¶]*Laboratoire de Physique des Solides, Université Paris-Saclay, CNRS, Université Paris-Sud, UMR 8502, 91405 Orsay, France.*

[§]*Laboratoire de Chimie, École Normale Supérieure de Lyon, 46 allée d'Italie, 69364 Lyon, France*

E-mail: Benjamin.Abecassis@ens-lyon.fr; Zeger.Hens@UGent.be

Abstract

The accurate determination of the dimensions of a nano-object is paramount to the development of nanoscience and technology. Here, we provide procedures for sizing quasi-spherical colloidal nanocrystals (NCs) by means of small-angle x-ray scattering (SAXS). Using PbS NCs as a model system, the protocols outline the extraction of the net NC SAXS pattern by background correction and address the calibration of scattered x-ray intensity to an absolute scale. Different data analysis methods are compared, and we show that they yield nearly identical estimates of the NC diameter in the case of a NC ensemble with a monodisperse and monomodal size distribution. Extending the analysis to PbSe, CdSe and CdS NCs, we provide SAXS calibrated sizing curves, which relate the NC diameter and the NC band-gap energy as determined using absorbance spectroscopy. In comparison with sizing curves calibrated by means of transmission electron microscopy (TEM), we

systematically find that SAXS calibration assigns a larger diameter than TEM calibration to NCs with a given band gap. We attribute this difference to the difficulty of accurately sizing small objects in TEM images. To close, we demonstrate that NC concentrations can be directly extracted from SAXS patterns normalized to an absolute scale, and we show that SAXS-based concentrations agree with concentration estimates based on absorption spectroscopy.

Keywords

Colloidal Nanocrystals, Small-Angle X-ray Scattering, Sizing Curves, Concentration

Introduction

The development of colloidal synthesis methods that result in the formation of semiconductor nanocrystals (NCs) with a narrow size dispersion and tunable sizes have turned these materials into model systems for nanoscience, with research interests covering diverse topics such as size quantization effects,[1–3] the chemistry of nanoscale surfaces,[4–6] and the self-assembly of nanoscale colloids.[7–9] In addition, they have been widely studied as alternative opto-electronic materials[10] that combine size- and surface-dependent optical and electronic properties[11,12] with a suitability for solution-based processing.[13–15] A general need faced by both scientific research on NCs and the further development of NC technology is the accurate determination of the average size of NCs in a given batch. NC sizing is, for example, essential to quantify size-dependent effects, and compare experimental results with theoretical predictions. Moreover, looking at the synthesis of NCs, both practical synthesis protocols and studies into nucleation and growth mechanisms rely on knowledge of the NC size, either to determine NC concentrations or to map the variation of the NC size throughout the reaction.[16,17] In addition, size and concentration are key quantities to know when applying NCs as biolabels,[18]

assessing NC toxicity,[19,20] or when simulating the functioning of NC-based opto-electronic devices.[21]

At present, the average diameter of NCs in a given batch is mostly determined by means of transmission electron microscopy (TEM). Operated in the most common, bright field mode, contrast in the 2D images results from a difference in mass and thickness between the sample and the carbon-film support. Therefore, the crystal regions of NCs will appear dark and this enables sizes to be determined by automated software packages, such as Digital Micrograph and ImageJ. Herein, particles are localized and measured by a variety of thresholding algorithms.[22] It should be noted that the interpretation of such images is often hampered by the simultaneous occurrence of the contrast-forming phenomena,[23] and that the particle-background boundary determination is prone to operator bias. In the particular case of semiconductor NCs or quantum dots, TEM imaging is typically used to construct calibration curves that relate the NC diameter to the energy of the band-edge transition. As this quantity is conveniently determined using absorbance spectroscopy, such so-called sizing curves make sizing straightforward, up to the point where it can be done in-situ.

Small-angle x-ray scattering (SAXS) is an alternative to determine NC diameters. As compared to TEM, SAXS has several advantages for the purpose of NC sizing. It is performed in solution, which makes that possibly detrimental drying artifacts, such as evaporation induced aggregation, can be avoided. Moreover, in a SAXS measurement, an ensemble of typically 10^6 particles is probed; a number that exceeds by 4 orders of magnitude the population adressed in a TEM analysis. Furthermore, analysis procedures induce little user bias. This point was recently made clear by a round-robin experiment,[24] in which the same sample was measured by different teams and their results were compared. Across the different laboratories, measured values of the mean radius and the polydispersity of a gold nanoparticle sample had an error below 1%, a result that confirms SAXS to be a very reliable technique to determine the size distribution of colloidal NCs.

In the case of semiconductor NCs, SAXS has been used for a long time to measure diameters.

One of the first papers reporting quantum confinement of CuCl in glass used SAXS to determine the size of the crystallites.[25] Later, Mattoussi *et al.*[26,27] used SAXS to investigated the interaction between CdSe NCs. Vossmeyer *et al.* used (powder) SAXS to assign diameters to different batches of CdS NCs, arguing that for small sizes TEM images were insufficiently clear.[28] For the few batches these authors analyzed both by TEM and SAXS – involving sub 4 nm CdS NCs – they systematically report TEM-based diameters that exceed SAXS-based diameters by 10 to 20%. Whereas several studies continued to use SAXS for the in-situ observation and analysis of NC nucleation and growth,[29] reports in which SAXS-based diameters are correlated with absorbance data to calibrate sizing curves are limited. A rare example is the study of Weidman and coworkers, who compared SAXS and TEM data obtained on PbS NCs.[30] Focusing on NC larger than 4.5 nm, they found that both approaches yield largely identical results. Grinolds *et al.* have also determined a sizing curve for 3 to 5.5 nm-sized PbS NCs using SAXS, and reported a significant deviation from previous findings.[31] For a given band-gap, they found that diameters estimated from SAXS measurements exceeded values calculated from TEM-based sizing curves. In both studies, the q-range was limited (0.07 to 0.4 Å^{-1} and 0.17 to 0.46 Å^{-1} for Weidman *et al.* and Grinolds *et al.* respectively).

These contradictory results and limited q-range motivated us to perform an in depth study on nanocrystal sizing by SAXS that involves both Pb- and Cd-based sulfides and selenides. For all these materials, colloidal synthesis methods cover a considerable range of diameters, and absorbance spectra exhibit a pronounced peak corresponding to band-edge transition. To make the method more accessible as an experimental technique for size and concentration determination, we first provide very detailed experimental methods and a step-by-step protocol for SAXS measurements, background correction and absolute intensity calibration. Next, focusing on a series of PbS QDs, we compare several methods to retrieve the diameter distribution from the SAXS patterns. These methods include direct fits of the SAXS curve using predefined distributions, next to a more recently developed Monte-Carlo approach that does

not start from an analytical expression of the diameter distribution. We show that all methods yield similar results for samples having a narrow and monomodal size distribution. For all four materials studied, this analysis yields a diameter that varies smoothly as a function of the NC band gap measured by means of absorbance spectroscopy. In the case of PbS and PbSe NCs, we find that the SAXS-based calibration of the sizing curve presented here, and previously published TEM-based calibrations coincides for larger NCs – typically with a diameter above 5 nm. Significant deviations, however, are observed for smaller NCs. In the case of zinc-blende CdSe NCs, where TEM-based sizing curves are limited to relatively small diameters, we find that the SAXS-based calibration yields systematically larger diameters than the previously published TEM-based calibration. In the case of CdS NCs, no such comparison is possible since no consistent, TEM-based sizing curve is available in the literature. Finally, we took the analysis of SAXS patterns one step further by showing that also NC concentrations can be determined reliably through SAXS. We thus provide compelling evidence that SAXS can be used as a preferred, quantitative method for size and concentration determination of dispersed NCs.

Materials and Methods

Colloidal Nanocrystals

For this work, we synthesized four series of CdS, CdSe, PbS and PbSe NCs with different diameters, using established hot-injection approaches as outlined in detail in Section 1 of the Supporting Information.[7,32–34] Figure 1 represents TEM images of representative samples from each series, showing that the batches used in this study are composed of quasi-spherical NCs with a narrow size dispersion. The latter conclusion is corroborated by the absorbance spectra of samples analysed by SAXS shown in Figure 2. These spectra feature a pronounced band-edge transition that gradually shifts to longer wavelengths with increasing nanocrystal diameter. To estimate the spectral position of these transitions, spectra were fitted to a set

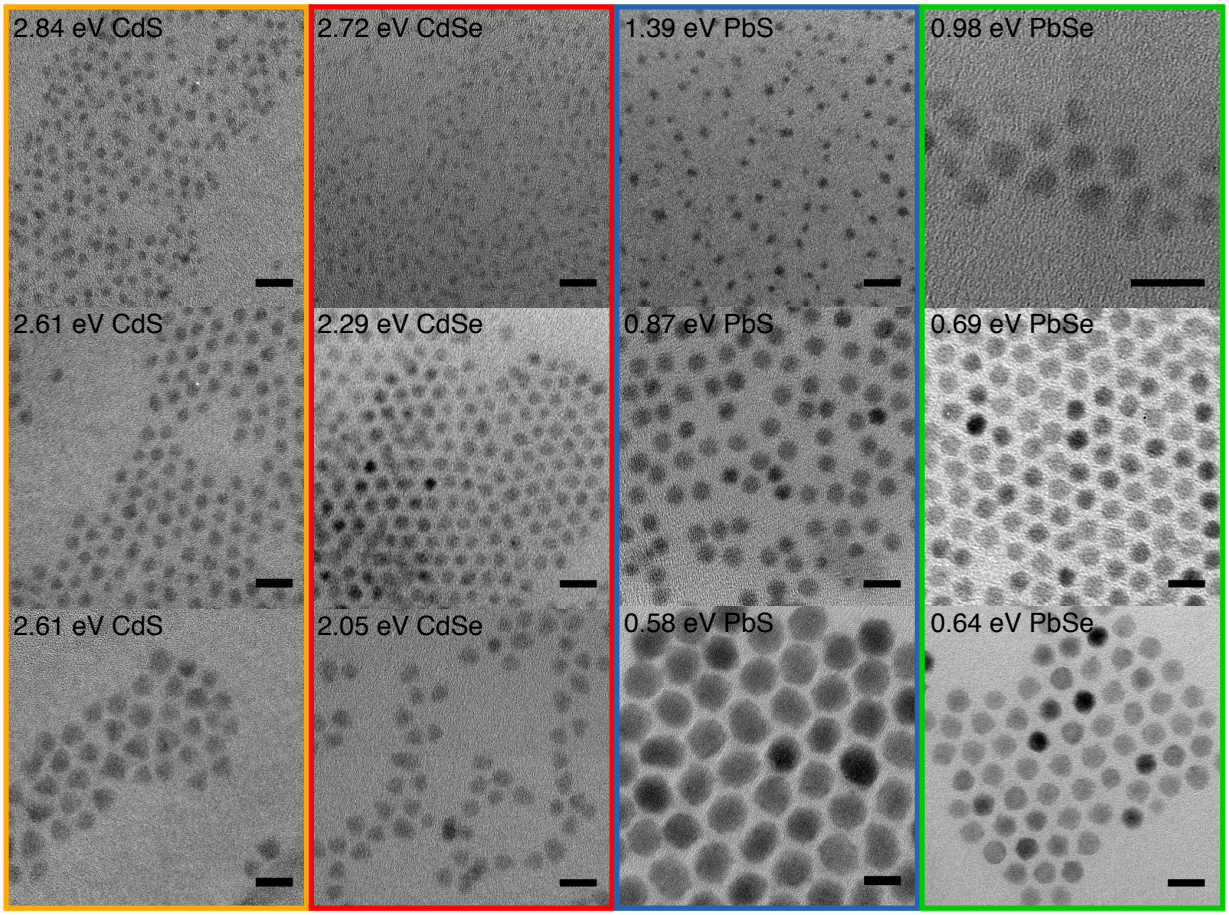

Figure 1: TEM micrographs of well-separated CdS(e) and PbS(e) NCs to illustrate the quasi-spherical shape of NCs.

of Gaussian peaks on top of a polynomial that accounted for the increasing background (see Supporting Information, Section 2.2). In what follows, the mean of the Gaussian that fits the band-edge transition will be used to construct sizing curves that relate the band-gap transition energy to the NC diameter.

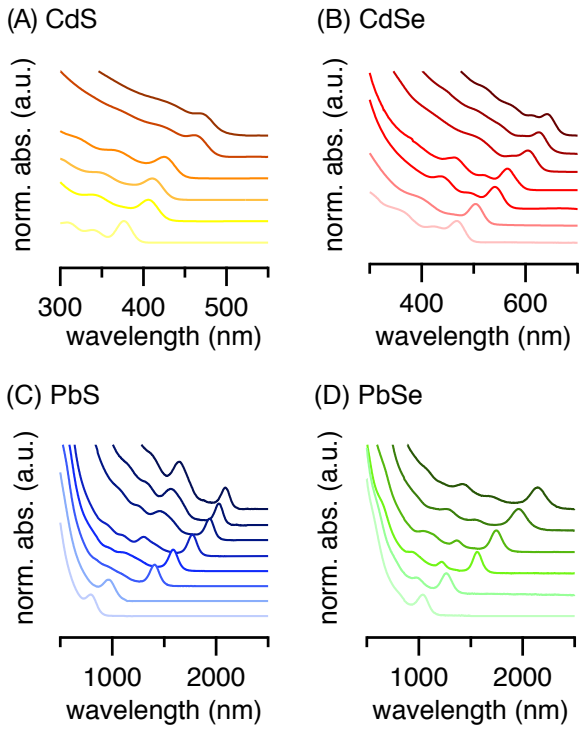

Figure 2: Typical (NIR)-UV-Vis absorbance spectra of (A) CdS, (B) CdSe, (C) PbS and (D) PbSe NCs, an offset is given for clarity.

Small Angle X-Ray Scattering

For characterization of NC dispersions using SAXS, 0.01 mm thin-wall glass capillaries were filled with a dispersion of NCs in toluene. In the case of PbS and PbSe, this procedure was carried out inside a nitrogen-filled glovebox. The capillaries were sealed with a UV-curable glue. Part of the synchrotron SAXS experiments were performed on the SWING beamline at the SOLEIL synchrotron (Saint-Aubin, France) using an x-ray energy of 8 keV and a sample to detector distance of 1 m. Other experiments were performed on the ID2 beamline at the ESRF

(Grenoble, France). In this case, the energy was 12 keV and the distance was comprised between 1 and 1.5 m. All the scattering patterns were radially averaged with beamline specific procedures to yield the intensity versus scattering vector q curve.

Procedures

Measuring SAXS patterns

SAXS measurements on NC dispersions can be performed in two ways (see Figure 3). First, one can load each sample in a separate glass capillary and use a capillary holder with multiple positions to measure several samples at a time (Figure 3A). The main advantage of this approach is throughput. With exposure times less than 1 seconds at a synchrotron, it is possible to measure tens of samples in hours. On the other hand, as capillaries will always have different thicknesses and background signals, measurements on an absolute scale are difficult. The alternative is to use a flow-through setup, which enables the scattering pattern of the empty capillary, the solvent and the solution to be measured at exactly the same spot in the capillary. By doing so, one ensures that exactly the right background signals are subtracted and the thickness of the sample can be measured very accurately through a secondary standard. Another advantage is that scattering patterns can be recorded on dispersions whilst flowing, an approach that limits possible radiation damage. Hence, from the point of view of SAXS data quality, flow setups are superior, yet they make for longer measurement times since the capillary must be carefully washed in between measuring two different dispersions.

The following describes a detailed protocol for measuring SAXS patterns that can be used to determine the size distribution and concentration of dispersed NCs. It is intended for researchers with a minimal hands-on experience of SAXS. First, we describe the preparation of capillaries. Next, it is outlined how to obtain a net NC SAXS pattern by radially averaging and correcting for the signal of the capillary and the solvent. Finally, we describe how a SAXS

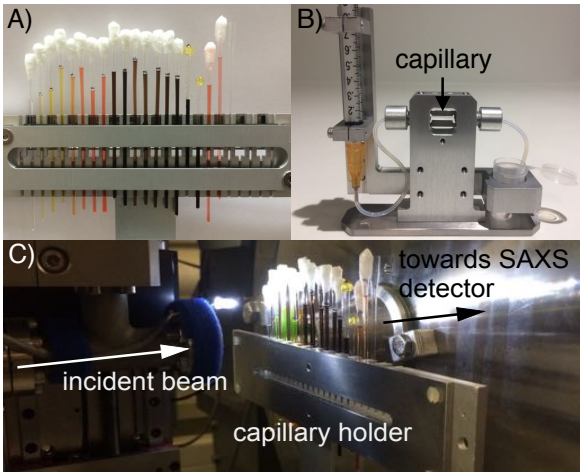

Figure 3: Illustration of the two different SAXS measurement procedures: A) using a series of capillaries and a capillary holder B) using a flow cell. This particular model was purchased from XENOCS. C) Beamline setup during SAXS experiments. The x-ray beam comes from the left, hits the sample and the scattered signal is detected by a camera.

diagram can be put on an absolute scale using standards.

Preparation of Capillaries

Caution. These glass capillaries are very thin and hence extremely fragile. Handle them with care to avoid their fracturing.

1. Use x-ray boro-silicate or quartz capillaries dedicated to xx-ray-ray experiments.

2. Fill the top of the capillary with 100 μL of the dispersion.

3. Make the dispersion flow at the bottom of the capillary by holding the top of the capillary with two fingers and make a fast circular move with your arm straight from top to bottom. Another option is to fill the capillary with a syringe equipped with a long and fine needle.

4. Close the top of the capillary to avoid evaporation of the solvent. We found that wrapping some Parafilm around the top of the glass capillary is enough to avoid significant evaporation for a few days. If there is a long time period between the capillary preparation and

the measurement, it is better to seal the capillary with a flame or UV-curable glue. The latter can be performed under nitrogen atmosphere for air-sensitive materials.

The procedure to subtract the solvent and capillary signal from the raw SAXS patterns vary with the measurement protocol. It is straightforward when a flow cell is used and it is done alongside the normalization at the absolute scale (see the corresponding section). When capillaries are used, the procedure is more complicated because the capillary signal has to be measured separately and the thickness of the capillary is not known precisely.

Radially averaging of raw SAXS patterns

In the case of isotropic samples (i.e. samples which do not display macroscopic orientation which is usually the case for nanoparticle dispersion) the SAXS intensity does not depend on the azimuthal angle on the detector and no information is lost by averaging the data over this angle. This azimuthal integration groups points with similar azimuthal angles into bins, yielding an intensity versus scattering vector q curve which is henceforth called the SAXS pattern (see Figure 4). This treatment, along with numerous other corrections[35] is usually performed by automated programs at the beam-line and we consider in the following that we deal with radially averaged $I(q)$ curves.

Calculation of Net NC SAXS Patterns when capillaries are used

1. Start from the SAXS patterns of the nanocrystal dispersion in a capillary I_{raw}^{disp}, the solvent in a capillary I_{raw}^{sol} and an empty capillary I^{cap}.

2. Obtain the net SAXS pattern I_{net}^{disp} of the dispersion by subtracting the patterns of the dispersion and the capillary.

$$I_{net}^{disp} = I_{raw}^{disp} - I^{cap} \tag{1}$$

Remark. This step is essential. The glass capillary yields a large SAXS signal at small q, where the scattered intensity increases quickly as q decreases. This is due to inho-

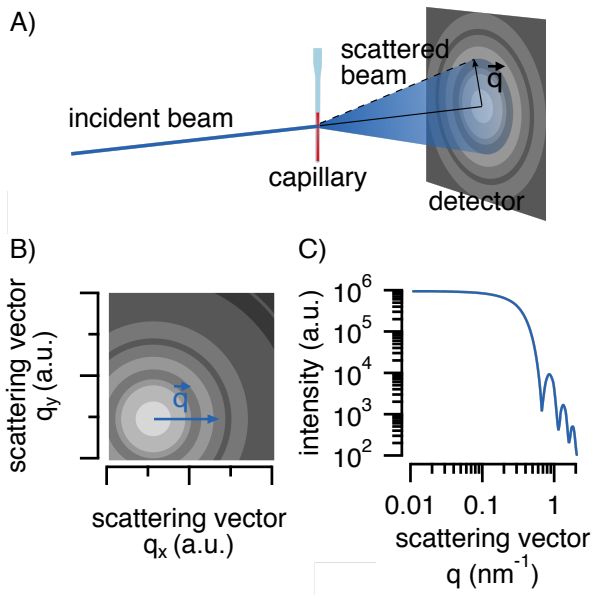

Figure 4: A) Illustration of the working principal of SAXS. The focused incident beam is scattered by the capillary and yields a pattern on the detector. B) As an example: simulated 2D pattern for spherical nanoparticles with a diameter of 14 nm and a polydispersity of 4.3 % and C) the corresponding 1D pattern $I(q)$ after radial averaging.

mogeneities in the glass. This signal gets much larger than that of the nanocrystals and dominates the overall intensity for small q. Hence it is important to subtract it from the signal.

Troubleshooting. Subtraction might not be perfect at small q because each capillary will have a different signal.

- When the signal of the empty cap is larger than the signal in which the NC solution is present, the aformentioned subtraction will lead to overcorrection. In that case, the only solution left is to crop the SAXS pattern and exclude the points where negative intensities are obtained. In this case, the q-range is reduced, only scattering intensities at larger q can be used, where the signal of the NC is significantly larger than that of the capillary.
- If the signal of the capillary is under-subtracted, an increasing scattering intensity at small q remains. This can be falsely attributed to an aggregation of nanoparticles,

which would also result in an increase of intensity at small q.

3. Subtract capillary from solvent:

$$I_{net}^{sol} = I_{raw}^{sol} - I^{cap} \tag{2}$$

4. Subtract solvent from the net dispersion to obtain the net NC SAXS pattern I_{net}^{NC} and divide by the capillary thickness provided by the capillary manufacturer e:

$$I_{net}^{NC} = I_{net}^{disp}/e_d - I_{net}^{sol}/e_s \tag{3}$$

Remark. Since different capillaries are used, their thicknesses can vary by 20%, whereas it must be known with a 1% accurary to get a neat subtraction at high q. Hence, our using of the symbols e_d and e_s to indicate thicknesses in Eq 3. To achieve a good subtraction under such conditions, we introduce a parameter x, plot the difference $I_{net}^{disp} - x \times I_{net}^{sol}$, and adjust x until the intensities of both signal are equal at high q. At large scattering vector the intensity of the nanoparticle is supposed to decrease like q^{-4} to become much smaller than the signal of the solvent which dominates the overall scattering signal. When we find the right x parameter, the thus obtained intensity is used as I_{net}^{NC} for further analysis. We usually find x values comprised between 0.8 and 1.2, a range that is consistent with thickness variation of around 20%.

Protocol for Obtaining SAXS Patterns on an Absolute Scale

To estimate the NC concentration from a SAXS pattern, the measured scattered intensity has to be normalized at an absolute scale. This needs further steps as described below. Apart from intensity normalization by means of a primary standard, which may or may not be a routine procedure at synchrotron beamlines, it also requires accurate knowledge of the sample thickness. For this, calibration measurements using a primary and a secondary standard with

the same cell are needed, which makes that absolute measurements are only possible with flow-cells.

1. Normalize the SAXS intensity using a standard such as glassy carbon.[36] Record a SAXS pattern of the standard (I^{st}) and tune a constant parameter c such that $c \times I^{st}$ yields exactly the same intensity as provided with the standard.

2. Using the flow cell, record the SAXS patterns (in that order) of (1) the empty capillary (I^{cap}), and (2) pure water (I^{w}_{raw}).

3. Obtain the net SAXS pattern of water as:

$$I^{w}_{net} = I^{w}_{raw} - I^{cap}$$

4. Find the thickness e of the water layer from the ratio of I^{w}_{net} and the absolute scattering intensity of water ($1.65\,10^{-3}\ \mathrm{mm}^{-1}$) at ambient temperature and pressure.[37]

5. Record the SAXS pattern of the solvent (I^{sol}_{raw}) and the NC dispersion (I^{disp}_{raw}).

6. Determine the absolute SAXS intensity for the NC dispersion and the solvent:

$$I^{disp}_{abs} = c \times \frac{I^{disp}_{raw}}{e}; I^{sol}_{abs} = \frac{I^{sol}_{raw}}{e}$$

7. Determine the absolute, net SAXS intensity of the NCs as (Figure 5):

$$I^{NC}_{net} = I^{disp}_{abs} - I^{sol}_{abs}$$

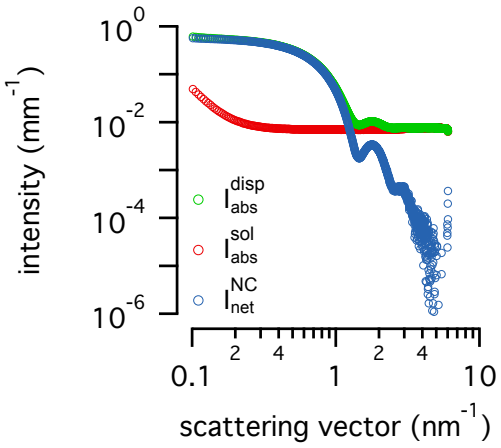

Figure 5: Typical SAXS patterns of a NC dispersion in a glass capillary (green), solvent in capillary (red) properly normalized at an absolute scale and the subtraction yielding the NC SAXS pattern to further analyze (blue).

Diameter determination by SAXS

General Approach

For size determination, NC dispersions loaded in separate capillaries were analyzed using synchrotron x-ray Small Angle Scattering. The 2D SAXS images were radially averaged using beamline specific procedures. Afterwards, the capillary and solvent signal are subtracted according using the protocol discussed above. The resulting net NC SAXS patterns were used for the size determination.

Figure 6 shows the SAXS pattern for a series of PbS NCs, which will be used as the reference system in this section. Qualitatively, the SAXS curves display a clear plateau at small scattering vectors (q). This indicates that the dispersion analyzed is stable and does not contain aggregated NCs, a result in line with the TEM observations shown in Figure 1. This ensures that we can neglect any structure factor in the SAXS analysis and consider a model of independent scatterers. With increasing q, the scattering intensity shows an abrupt decrease, followed by several intensity oscillations. This indicates that the samples contain highly monodisperse nanocrystal ensembles.

For the quantitative analysis of the SAXS pattern, we start from the assumption that such

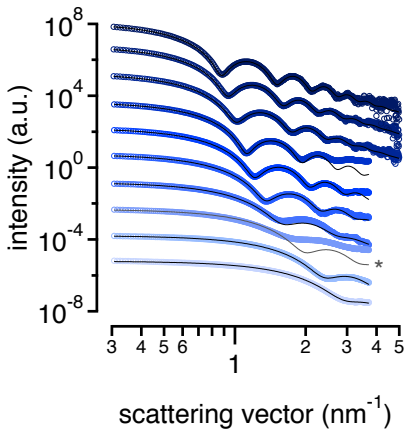

Figure 6: Experimental SAXS patterns for 1.55-0.59 eV PbS NCs (open circles), fitted by means of a Gaussian mono-modal size distribution (line).

samples of PbS NCs consist of spheres of homogeneous electron density, dispersed in a solvent. The SAXS intensity on an absolute scale I is then given by:[38,39]

$$I(q) = n(\Delta\rho)^2 \int_0^\infty V(R)^2 D(R) P(q,R) dR, \tag{4}$$

Here, n is the NC concentration, $\Delta\rho$ is the difference of scattering length density between the NCs and the solvent (the contrast), $V(R)$ is the volume of a sphere of radius R, $D(R)$ is the radius distribution and $P(q,R)$ is the form factor of a sphere. Equation 4 makes clear that the shape of the SAXS curve only depends on the NC radius distribution $D(R)$, whereas the overall intensity is dictated by the NC concentration n. Hence, descriptors such as the average diameter and the size dispersion can be obtained from an intensity versus q signal in arbitrary units (a.u.), whereas a precise measure of the NC concentration requires absolute intensities. In essence, two different methods can be used to retrieve the radius distribution from the SAXS pattern. First of all, one could fit the experimental spectrum to an intensity pattern simulated using Eq 4 by means of a parametrized analytical distribution function. Alternatively, the mean diameter and the size dispersion can be estimated by means of Monte-Carlo (MC) simulations,[40] which extract a volume-weighted size distribution from the SAXS pattern. In what follows, we compare both approaches by means of PbS NC SAXS patterns shown in

Figure 6.

Diameter Analysis Using Presupposed Analytical Distributions

To assess the stability of the diameter estimation using a presupposed distribution function, we evaluated SAXS patterns obtained on PbS QDs using a Gaussian, a Schulz and a Log-Normal distribution. These respective distributions were parameterized as indicated in Table 1, while the expressions for the NC size disperion can be found in Section 3 of the Supporting Information.

Table 1: Expressions of Gaussian, Log-normal and Schulz distribution functions.

Distribution	**Expression for** $D(R)$
Gaussian	$\frac{1}{\sqrt{2\pi}\sigma} e^{-\frac{(R-R_0)^2}{2\sigma^2}}$
Schulz	$\left(\frac{R}{R_0}\right)^Z (Z+1)^{(Z+1)} \frac{e^{-(Z+1)} R/R_0}{\Gamma(Z+1)}$
Lognormal	$\frac{1}{R\sigma\sqrt{2\pi}} \exp\left(-\frac{(\ln R-\mu)^2}{2\sigma^2}\right)$

R = radius; R_0 = mean radius; σ = standard deviation; $\Gamma(z) = \int_o^\infty t^{z-1} e^{-t} dt$

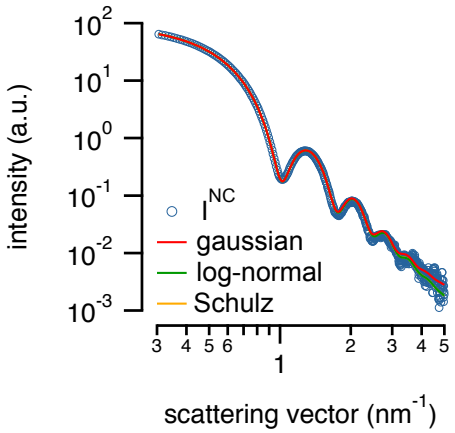

Figure 7: Fitting of a PbS NC SAXS pattern with a model of polydisperse spheres for different mathematical form of the distribution: gaussian, log-normal or Schulz. The three fits are excellent and indistinguishable.

As indicated by the example shown in Figure 7, the best fits of the SAXS pattern using either of these distributions superpose, and can not be distinguished. Furthermore, all the fits are

excellent, except for the sample with a band gap of 0.99 eV, which is the pattern marked with $*$ in Figure 6. In line with the coinciding fits, we found that the estimates of the mean diameter and the size dispersion do not depend on the actual analytical expression of the distribution. As can be seen from Table 2, the mean diameter is the same within 0.02 nm and the differences on the size dispersion are also very small. This indicates that these values are robust and do not depend on the actual radius distribution that was put forward. A detailed fitting protocol using the software package 'SASView' can found in Section 3.1 of the Supplementary Information.

Table 2: Results from different fitting procedures for the PbS NC series. For each fitting method, the mean diameter (d) and the polydispersity (poly.) is indicated. The mathematical expression of the different size distributions is described in Table 1.

Gaussian		**Log-Normal**		**Schulz**		**Monte-Carlo**	
d (nm)	poly. (%)	d (nm)	poly. (%)	d (nm)	poly. (%)	d (nm)	poly. (%)
2.86	17.13	2.84	17.46	2.86	18.47	3.16	18.04
3.62	12.02	3.61	11.56	3.62	12.33	3.77	13.21
4.22	18.22	4.21	18.23	3.94	35.26	4.45	25.96
5.34	14.38	5.36	12.62	5.38	13.09	5.45	20.45
6.58	8.13	6.56	7.89	6.58	7.96	6.68	10.33
7.34	7.23	7.33	7.04	7.35	7.09	7.43	8.96
7.99	5.51	7.98	5.40	7.99	5.42	8.06	5.48
8.74	7.19	8.73	7.04	8.75	7.09	8.88	7.00
9.53	6.53	9.52	6.41	9.53	6.45	9.65	4.81
10.12	5.79	10.12	5.55	10.13	5.57	10.20	6.39

Monte Carlo Analysis of Scattering Patterns

Next, we applied the Monte-Carlo approach as developed by Bressler *et al.* to fit the SAXS patterns of the PbS NCs series. In this method, no particular shape of the radius distribution is assumed. Even so, we found that all the size distribution retrieved by this method for our samples are monomodal, a result that is consistent with the excellent fits found with presupposed distributions. The mean diameters retrieved by MC are slightly higher, probably because a volume weighted size distribution is obtained instead of a number weighted size distribution.
An interesting case to compare both approaches is the SAXS pattern recorded on the 0.99 eV sample of the PbS series, which emerged as an outlier in Figure 6 (marked with $*$). A closer

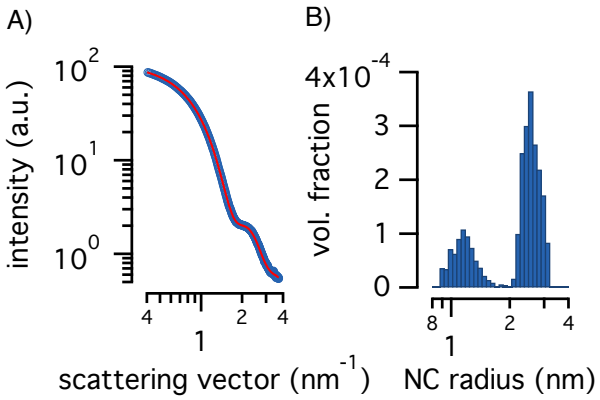

Figure 8: Result of the Monte-Carlo fitting of the outlier PbS sample. Note the bi-modal distribution with a maximum at 1.5 nm and a second maximum at 2.1 nm.

examination of the SAXS pattern and the associated fits based on presupposed distributions, shows that all these monomodal distributions underestimate the SAXS intensity at high q. When the Monte-Carlo approach is used instead (Figure 8), the retrieved size distribution appears as bi-modal with a population of small particles that have a mean radius of around 1.5 nm appearing alongside the main population with a mean radius 2.1 nm. Possibly, this population of smaller nanoparticles corresponds to unbound lead oleate molecules which are still present due to insufficient purification. Note that the Monte-Carlo approach yields a correct fit of the SAXS intensity at high q (Figure 8A).

Error estimation

The comparison of descriptor estimation in the case of the PbS series shows that all the methods studied yield essentially the same mean diameter and size dispersion. Apart from the error on these estimates that comes with a given fitting method, we identify two other sources of uncertainty in our measurements. The first one is the overall error on the SAXS measurement of a given sample. This includes the measurement itself, and all the data treatment procedures. These errors have been shown to impact the final mean radius and polydispersity by less than 1%.[35] The other uncertainty is that of the choice of fitting procedure (least square fit or Monte-Carlo). Our data show that this error is even smaller and is well below 1%. Hence,

the dominating uncertainty of our measurement lies in the SAXS modeling choice. When the fit for a monomodal size distribution is excellent, which is the case for large nanoparticles where multiple oscillations are visible, this error is a few percent at a maximum. Only for smaller particles, such as the first of the PbS series, the uncertainty is higher, yet it remains within the 10% range. Most likely, this increased error is caused by the solvent scattering masking the oscillations of the scattered intensity by the NCs at high q.

SAXS-Calibrated Sizing Curves

SAXS Analysis of PbSe, CdSe and CdS Dispersions

A major result of the analysis of the SAXS patterns recorded on PbS dispersions is that very similar NC descriptors are obtained, regardless of the fitting methodology. We therefore extended the SAXS study to PbSe, CdSe and CdS NCs, where we restricted ourselves to a data analysis based on Gaussian distributions. All experimental patterns, and Gaussian fits are shown in Figure 9. The thus obtained estimates for the NC diameter and the size dispersion have been summarized in the Supporting Information (Table S2).

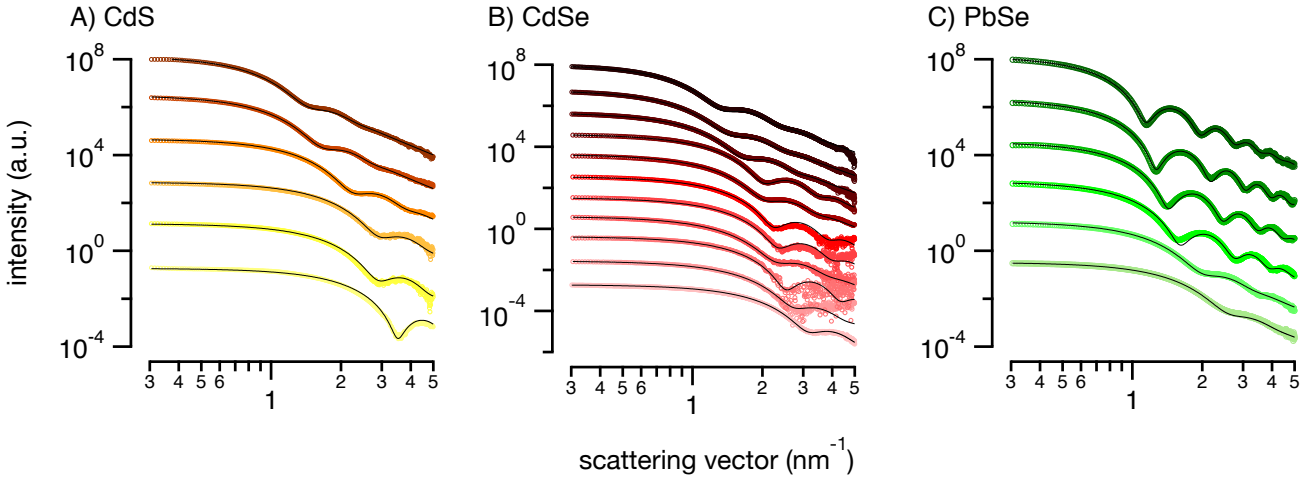

Figure 9: Experimental SAXS patterns for (A) 3.3-2.6 eV CdS, (B) 2.6-1.9 eV CdSe, (C) 1.2-0.6 eV PbSe NCs (open circles) with Gaussian size distribution (line).

SAXS-Based Sizing Curves for PbS, PbSe, CdS and CdSe Nanocrystals

Having an estimated NC diameter d_{NC} from SAXS and the optical band gap E_g from absorbance measurements, we can construct calibration curves that link both quantities. Figure 10 displays the resulting sizing curves, where each marker represents an experimental (d, E_g) data point and each trend line is an interpolation determined by fitting the set of data points to the empirical expression:

$$E_g = E_{g,bulk} + \frac{1}{a + b.d_{NC} + c.d_{NC}^2} \tag{5}$$

Here, $E_{g,bulk}$ stands for the bulk band gap of the material and a,b and c are fitting parameters. These parameters are summarized in Table 3 for all 4 materials, together with their bulk band gap and the energy range in which the sizing curve is valid. All experimental data points are in good agreement with the final sizing curve, clearly demonstrating the high reliability of SAXS to determine NC diameters. For practical considerations, a straightforward relation between d_{NC} and the wavelength of the band-edge transition is often useful. Such relations are given in the Supporting Information (Section 5).

Table 3: Empirical fitting parameters of SAXS-based sizing curves (Equation 5) with bulk band gap and energy range.

	CdS	CdSe	PbS	PbSe
$a\,(\mathrm{eV}^{-1})$	-1.123	0.756	0.0261	-0.891
$b\,(\mathrm{nm}^{-1}\cdot\mathrm{eV}^{-1})$	0.768	-0.249	0.235	0.621
$c\,(\mathrm{nm}^{-2}\cdot\mathrm{eV}^{-1})$	0.0522	0.139	-	-0.0141
$E_{g,bulk}\,(\mathrm{eV})$	2.42	1.74	0.41	0.278
$E_{g,max} - E_{g,min}\,(\mathrm{eV})$	3.29-2.62	2.64-1.93	1.55-0.59	1.19-0.58

Concentration determination by SAXS

Next to the NC diameter, the NC concentration is a second key descriptor of NC dispersions. Currently, such concentrations are determined by combining estimates of the NC diameter and the total volume of semiconductor material in a dispersion. The former is often calculated from

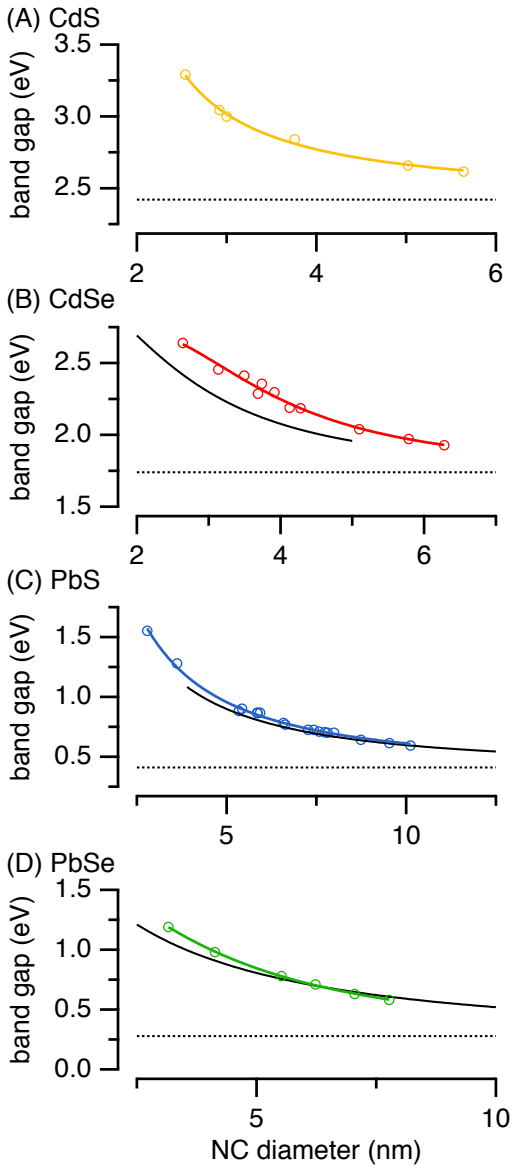

Figure 10: Relation between the band gap and the diameter for (A) CdS, (B) CdSe, (C) PbS and (D) PbSe NCs. To the the set of SAXS data (open circles), a sizing curve is fitted (colored line). The black lines represent a TEM-based sizing curves from literature,[41–43] while the dotted line denotes the bulk band gap.

the energy of the band-edge transition by means of a sizing curve, whereas the latter can be obtained from the absorbance of the dispersion at energies well above the band-edge transition. For many materials, the absorption coefficient μ_i at these higher energies is constant, and agrees with a theoretical value that can be calculated based on bulk optical properties.[44] Combining both elements yields a molar absorption coefficient ϵ as (N_A: Avogadro's number):

$$\epsilon = \frac{\pi . d_{NC}^3}{6} \frac{N_A . \mu_i}{ln(10)} \tag{6}$$

Having ϵ at hand, the molar concentration of NCs c_{NC} is readily obtained from the absorbance A of the disperion by means of the Lambert-Beer law (L: sample length):

$$c = \frac{A}{\epsilon . L}$$

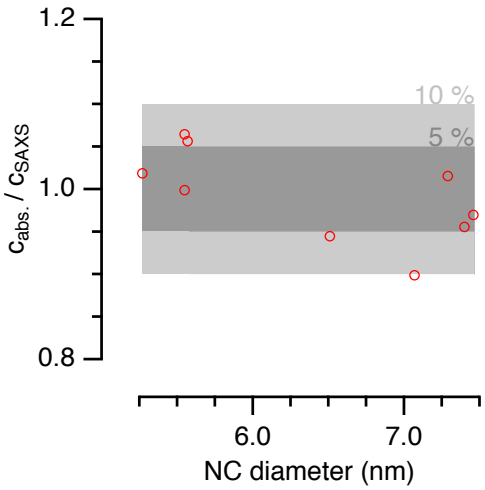

Figure 11: Ratio of PbS NC concentration determined by conventional method (abs.) and directly by SAXS.

Equation 4 suggests that SAXS provides an alternative to determine the NC concentration as the scattered x-ray intensity is directly proportional to the NC concentration. Hence, when special care is taken to normalize the intensity on an absolute scale, the NC concentration should

follow directly from the intensity limit when $q \to 0$. As outlined in the protocol section, such absolute measurements involve a judicious calibration procedure that relies on an accurate knowledge of the sample thickness. To assess the accuracy of this approach, we measured SAXS patterns for a series of PbS NCs with a flow cell and determined the NC concentration from the thus obtained absolute scattering intensity. In addition, the same dispersions were analyzed using absorbance spectroscopy, and the NC molar concentration was determined from their absorbance at 400 nm according to literature.[41]

Figure 11 shows the ratio of the NC concentration determined by absorbance spectroscopy and SAXS on a sample-by-sample basis. For all samples, these ratios fall randomly within a band of $\pm 10\%$ around the expected value of 1. A striking result since two completely different approaches were used to determine the same quantity. This indicates that SAXS is a viable alternative method for concentration determination and therefore can be useful in future fundamental studies concerning nucleation and growth mechanisms of NC syntheses.

Discussion

The overview of the SAXS-based sizing curves given in Figure 10 enables us to compare SAXS and TEM as methods to calibrate nanocrystal sizing curves. As compared to TEM-based curves,[41–43] we find that in the case of PbS and PbSe NCs larger than $\sim 5\,\mathrm{nm}$, both methods yield coinciding sizing curves. For smaller diameters, however, we find that SAXS calibration always assigns a larger diameter to a given band-edge energy then TEM calibration. This trend points towards systematic, size-dependent deviations between both techniques. Most likely, this differences are due to TEM-based calibrations underestiming the actual NC diameter due to a poor electron scattering contrast between small NCs and the underlying amorphous carbon-film support. This will lead to a low pixel intensity difference at the particle-support boundary that jeopardizes factual particle edge determination for very small NCs. Moreover, the fractional contribution of a single pixel will become substantial, leading to large

errors if misinterpreted.[22] If indeed limited contrast induces errors in TEM-based sizing, the problem such be more pronounced for materials giving weaker contrast, i.e., materials composed of small atomic number elements. This effect is clearly noticeable in the case of CdSe NCs, where we find a considerable larger underestimation of the NC diameter by TEM.

A full quantification of TEM-induced errors is not possible since instrumental parameters like magnification, Cs-correction and contrast transfer function can all have a strong influence on the edge determination. Moreover, the user-dependent character of the data analysis further decreases the reliability of TEM for sizing, especially for small and light-element NCs. To counterbalance such effects, imaging is better done in an aberration corrected microscope in higher magnification conditions, and, if possible, using high contrast techniques such as high angle annular dark field (HAADF) scanning TEM (STEM). In this latter case, one would be able to enhance the particle-support contrast ratio, and have a clear and sharp definition of the quantum dot contour, achieving even atomic column definition. Nevertheless, sampling of an inadequate number of particles,[45] and the inevitable increase in electron flux causing beam damage, can still induce errors. SAXS, on the other hand, does not have such limitation, which makes it most likely the more reliable technique for size calibration over the complete size range analyzed here.

Conclusions

We have proposed protocols for the sizing of dispersed nanocrystals by means of small angel x-ray scattering. Using dispersions of PbS nanocrystals of different sizes as a reference material, we show that in the case of monodisperse nanocrystal batches, data analysis by means of a parameterized analytical radius distribution or a Monte Carlo approach that does not use a presupposed expression for the radius distribution yield coinciding results. We extended the study to PbSe, CdSe and CdS nanocrystal dispersions, and present so-called sizing curves for these materials in which the band-edge energy is related to the nanocrystal diameter by

means of SAXS calibration. We show that in the case of sub 5 nm nanocrystals, a similar calibration using TEM imaging systematically yields smaller diameters for a given band-edge energy, a difference we assign to the difficulty to delineate the nanocrystal boundary in case of low-contrast TEM images. Finally, we show that SAXS patterns calibrated to an absolute scale can be used to estimate nanocrystal concentrations, providing values that differ by less than 10 % deviation from concentrations obtained using absorbance spectroscopy. We conclude that SAXS is a most reliable and versatile technique for the quantitative analysis of the diameter and concentration of dispersed nanocrystals, that may become a mainstream analysis method in nanocrystal science thanks to the analysis protocols and reference data provided here.

Acknowledgement

We are grateful to J. Perez and T. Bizien for assistance during beamtime and to the SOLEIL staff for smoothly running the facility. We thank ESRF for provision of the beamtime and S. Prevost for help during the measurements. We appreciate the scientific discussions concerning imaging of nanocrystals by transmission electron microscopes with Jordi Arbiol. Z.H. acknowledges Ghent University (GOA 01G01513) for funding. Benjamin, do you want to include some fundings?

Supporting Information Available

The Supplementary Information contains detailled NC synthesis methods, an example of absorption spectra fitting (Igor Pro) and SAXS patterns (SASView), datapoints of sizing curves and alternative sizing curves, relating the NC diameter to the wavelength of the first optical transition.

This material is available free of charge via the Internet at `http://pubs.acs.org/`.

References

(1) Murray, C. B.; Norris, D. J.; Bawendi, M. G. Synthesis and characterization of nearly monodisperse CdE (E = sulfur, selenium, tellurium) semiconductor nanocrystallites. *Journal of the American Chemical Society* **1993**, *115*, 8706–8715.

(2) Alivisatos, A. P. Semiconductor Clusters, Nanocrystals, and Quantum Dots. *Science* **1996**, *271*, 933–937.

(3) Murray, C. B.; Kagan, C. R.; Bawendi, M. G. Synthesis and Characterization of Monodisperse Nanocrystals and Close-Packed Nanocrystal Assemblies. *Annual Review of Materials Science* **2000**, *30*, 545–610.

(4) Nag, A.; Kovalenko, M. V.; Lee, J.-S.; Liu, W.; Spokoyny, B.; Talapin, D. V. Metal-free Inorganic Ligands for Colloidal Nanocrystals: S_2^{2-}, HS^-, Se^{2-}, HSe^-, Te^{2-}, HTe^-, TeS_3^{2-}, OH^-, and NH_2^- as Surface Ligands. *Journal of the American Chemical Society* **2011**, *133*, 10612–10620.

(5) Anderson, N. C.; Hendricks, M. P.; Choi, J. J.; Owen, J. S. Ligand Exchange and the Stoichiometry of Metal Chalcogenide Nanocrystals: Spectroscopic Observation of Facile Metal-Carboxylate Displacement and Binding. *Journal of the American Chemical Society* **2013**, *135*, 18536–18548.

(6) Hens, Z.; Martins, J. C. A Solution NMR Toolbox for Characterizing the Surface Chemistry of Colloidal Nanocrystals. *Chemistry of Materials* **2013**, *25*, 1211–1221.

(7) Murray, C. B.; Sun, S.; Gaschler, W.; Doyle, H.; Betley, T. A.; Kagan, C. R. Colloidal synthesis of nanocrystals and nanocrystal superlattices. *IBM Journal of Research and Development* **2001**, *45*, 47–56.

(8) Evers, W.; Goris, B.; Bals, S.; Casavola, M.; de Graaf, J.; van Roij, R.; Dijkstra, M.; Vanmaekelbergh, D. Low-Dimensional Semiconductor Superlattices Formed by Geometric Control over Nanocrystal Attachment. *Nano Letters* **2012**, *13*, 2317–2323.

(9) Shevchenko, E. V.; Talapin, D. V.; Kotov, N. A.; O'Brien, S.; Murray, C. B. Structural diversity in binary nanoparticle superlattices. *Nature* **2006**, *439*, 55 –59.

(10) Kovalenko, M. V. et al. Prospects of Nanoscience with Nanocrystals. *ACS Nano* **2015**, *9*, 1012–1057.

(11) Giansante, C.; Infante, I.; Fabiano, E.; Grisorio, R.; Suranna, G. P.; Gigli, G. "Darker-than-Black" PbS Quantum Dots: Enhancing Optical Absorption of Colloidal Semiconductor Nanocrystals via Short Conjugated Ligands. *Journal of the American Chemical Society* **2015**, *137*, 1875–1886.

(12) Brown, P. R.; Kim, D.; Lunt, R. R.; Zhao, N.; Bawendi, M. G.; Grossman, J. C.; Bulović, V. Energy Level Modification in Lead Sulfide Quantum Dot Thin Films through Ligand Exchange. *ACS Nano* **2014**, *8*, 5863–5872.

(13) McDonald, S. A.; Konstantatos, G.; Zhang, S.; Cyr, P. W.; Klem, E. J. D.; Levina, L.; Sargent, E. H. Solution-processed PbS quantum dot infrared photodetectors and photovoltaics. *Nature Materials* **2005**, *4*, 1012–1057.

(14) Kim, J. Y.; Voznyy, O.; Zhitomirsky, D.; Sargent, E. H. 25th Anniversary Article: Colloidal Quantum Dot Materials and Devices: A Quarter-Century of Advances. *Advanced Materials* **2013**, *25*, 4986–5010.

(15) Yuan, M.; Liu, M.; Sargent, E. H. Colloidal quantum dot solids for solution-processed solar cells. *Nature Energy* **2016**, *1*.

(16) Owen, J. S.; Chan, E. M.; Liu, H.; Alivisatos, A. P. Precursor Conversion Kinetics and

the Nucleation of Cadmium Selenide Nanocrystals. *Journal of the American Chemical Society* **2010**, *132*, 18206–18213.

(17) Abe, S.; Capek, R. K.; De Geyter, B.; Hens, Z. Reaction Chemistry/Nanocrystal Property Relations in the Hot Injection Synthesis, the Role of the Solute Solubility. *ACS Nano* **2013**, *7*, 943–949.

(18) Bruchez, M.; Moronne, M.; Gin, P.; Weiss, S.; Alivisatos, A. P. Semiconductor Nanocrystals as Fluorescent Biological Labels. *Science* **1998**, *281*, 2013–2016.

(19) Alkilany, A. M.; Murphy, C. J. Toxicity and cellular uptake of gold nanoparticles: what we have learned so far? *Journal of Nanoparticle Research* **2010**, *12*, 2313–2333.

(20) Elsaesser, A.; Howard, C. V. Toxicology of nanoparticles. *Advanced Drug Delivery Reviews* **2012**, *64*, 129–137.

(21) Xie, W.; Zhu, Y.; Bisschop, S.; Aubert, T.; Hens, Z.; van Thourhout, D.; Geiregat, P. Colloidal Quantum Dots Enabling Coherent Light Sources for Integrated Silicon-Nitride Photonics. *IEEE Journal of Selected Topics in Quantum Electronics* **2017**, *23*, 1–13.

(22) Pyrz, W. D.; Buttrey, D. J. Particle Size Determination Using TEM: A Discussion of Image Acquisition and Analysis for the Novice Microscopist. *Langmuir* **2008**, 11350–11360.

(23) Chattopadhyay, K.; Banerjee, A. *An Introduction to Nanoscience and Nanotechnology*; PHI Learning, 2009.

(24) Pauw, B. R.; Kästner, C.; Thünemann, A. F. Nanoparticle size distribution quantification: results of a small-angle X-ray scattering inter-laboratory comparison. *Journal of Applied Crystallography* **2017**, *50*, 1280–1288.

(25) Golubkov, V.; Ekimov, A. I.; Onushchenko, A. A.; Tsekhomskii, V. Growth kinetics of CuCl microcrystals in a glassy matrix. *Glass Physics and Chemistry (Fizika i Khimiya Stekla)* **1981**, *7*, 397–401.

(26) Mattoussi, H.; Cumming, A. W.; Murray, C. B.; Bawendi, M. G.; Ober, R. Characterization of CdSe nanocrystallite dispersions by small angle x-ray scattering. *The Journal of Chemical Physics* **1996**, *105*, 9890–9896.

(27) Mattoussi, H.; Cumming, A. W.; Murray, C. B.; Bawendi, M. G.; Ober, R. Properties of CdSe nanocrystal dispersions in the dilute regime: Structure and interparticle interactions. *Physical Review B* **1998**, *58*, 7850–7863.

(28) Vossmeyer, T.; Katsikas, L.; Gienig, M.; Popovic, I. G.; Diesner, K.; Chemseddine, A.; Eychmiiller, A.; Weller, H. CdS Nanoclusters: Synthesis, Characterization, Size Dependent Oscillator Strength, Temperature Shift of the Excitonic Transition Energy, and Reversible Absorbance Shift. *Journal of Physical Chemistry* **1994**, 7665–7673.

(29) Abécassis, B.; Bouet, C.; Garnero, C.; Constantin, D.; Lequeux, N.; Ithurria, S.; Dubertret, B.; Pauw, B. R.; Pontoni, D. Real-Time in Situ Probing of High-Temperature Quantum Dots Solution Synthesis. *Nano Letters* **2015**, *15*, 2620–2626.

(30) Weidman, M. C.; Beck, M. E.; Hoffman, R. S.; Prins, F.; Tisdale, W. A. Monodisperse, Air-Stable PbS Nanocrystals via Precursor Stoichiometry Control. *ACS Nano* **2014**, *8*, 6363–6371.

(31) Grinolds, D. D. W.; Brown, P. R.; Harris, D. K.; Bulovic, V.; Bawendi, M. G. Quantum-Dot Size and Thin-Film Dielectric Constant: Precision Measurement and Disparity with Simple Models. *Nano Letters* **2015**, *15*, 21–26.

(32) Abe, S.; Capek, R. K.; De Geyter, B.; Hens, Z. Tuning the Postfocused Size of Colloidal Nanocrystals by the Reaction Rate : From Theory to Application. *ACS Nano* **2012**, 42–53.

(33) Flamee, S.; Cirillo, M.; Abe, S.; De Nolf, K.; Gomes, R.; Aubert, T.; Hens, Z. Fast, high yield, and high solid loading synthesis of metal selenide nanocrystals. *Chemistry of Materials* **2013**, *25*, 2476–2483.

(34) Hendricks, M. P.; Campos, M. P.; Cleveland, G. T.; Jen-La Plante, I.; Owen, J. S. A tunable library of substituted thiourea precursors to metal sulfide nanocrystals. *Science* **2015**, *348*, 1226–1230.

(35) Pauw, B. R. Everything SAXS: small-angle scattering pattern collection and correction. *Journal of Physics: Condensed Matter* **2013**, *25*, 383201.

(36) Zhang, F.; Ilavsky, J.; Long, G. G.; Quintana, J. P. G.; Allen, A. J.; Jemian, P. R. Glassy Carbon as an Absolute Intensity Calibration Standard for Small-Angle Scattering. *Metallurgical and Materials Transactions A* **2010**, *41*, 1151–1158.

(37) Dreiss, C. A.; Jack, K. S.; Parker, A. P. On the absolute calibration of bench-top small-angle X-ray scattering instruments: a comparison of different standard methods. *Journal of Applied Crystallography* **2006**, *39*, 32–38.

(38) Guinier, A.; Fournet, G. *Small-angle scattering of X-rays*; Wiley, 1955; bibtex: guinier_small-angle_1955.

(39) Als-Nielsen, J.; McMorrow, D. *Elements of modern x-ray physics*; Wiley: New York, NY, 2001; bibtex: Als-Nielsen2001.

(40) Bressler, I.; Pauw, B. R.; Thünemann, A. F. *McSAS* : software for the retrieval of model parameter distributions from scattering patterns. *Journal of Applied Crystallography* **2015**, *48*.

(41) Moreels, I.; Lambert, K.; Smeets, D.; De Muynck, D.; Nollet, T.; Martins, J. C.; Vanhaecke, F.; Vantomme, A.; Delerue, C.; Allan, G.; Hens, Z. Size-dependent optical properties of colloidal PbS quantum dots. *ACS Nano* **2009**, *3*, 3023–3030.

(42) Capek, R. K.; Moreels, I.; Lambert, K.; Muynck, D. D.; Zhao, Q.; Tomme, V.; Vanhaecke, F.; Hens, Z. Optical Properties of Zincblende Cadmium Selenide Quantum Dots. *Journal of Physical Chemistry C* **2010**, 6371–6376.

(43) Moreels, I.; Lambert, K.; Muynck, D. D.; Vanhaecke, F.; Poelman, D.; Martins, J. C.; Allan, G.; Hens, Z. Composition and Size-Dependent Extinction Coefficient of Colloidal PbSe Quantum Dots. *Chemistry of Materials* **2007**, 6101–6106.

(44) Hens, Z.; Moreels, I. Light Absorption by Colloidal Semiconductor Quantum Dots. *Journal of Materials Chemistry* **2012**, *22*, 10406–10415.

(45) Murphy, C. J.; Buriak, J. M. Best Practices for the Reporting of Colloidal Inorganic Nanomaterials. *Chemistry of Materials* **2015**, *27*, 4911–4913.

Graphical TOC Entry